Evolution of specific interface area in dendritic alloy solidification

2015 IOP Conf. Ser.: Mater. Sci. Eng. 84 012072

(http://iopscience.iop.org/1757-899X/84/1/012072)

Evolution of specific interface area in dendritic alloy solidification

H Neumann-Heyme[1] K Eckert[1] and C Beckermann[2]

[1] Institute for Fluid Dynamics, Technische Universität Dresden, 01062 Dresden, Germany
[2] Department of Mechanical and Industrial Engineering, The University of Iowa, Iowa City, IA 52242, USA

E-mail: hieram.neumann-heyme@tu-dresden.de

Abstract. The specific area of the solid-liquid interface is an important integral measure for the morphological evolution during solidification. It represents not only the inverse of a characteristic length scale of the microstructure, but it is also a key ingredient in volume-averaged models of alloy solidification. Analytical descriptions exist for either pure coarsening or pure growth processes. However, all alloy solidification processes involve concurrent growth and coarsening. In the present study, the kinetics of the solid-liquid interface of a columnar dendrite are studied using a 3D phase-field model. The simulation results are combined with data from recent experiments to study the influence of the cooling rate on the evolution of the interfacial area.

1. Introduction

A key aspect in predicting the microstructure in castings is the detailed knowledge of how geometrical features evolve over time during solidification. Often, local features, such as the secondary dendrite arm spacing, are used for the geometrical characterization of the microstructure. However, they represent incomplete descriptions of the solid structure and their measurement can become difficult during the late stages of solidification, when the structure undergoes fundamental transformations. Alternatively, integral measures, such as the specific area of the solid-liquid interface, can be introduced that more generally characterize the overall morphology [1, 2]. One definition of the specific interface area is the amount of interface area A per volume of the enclosed solid phase V_s,

$$S_s = A/V_s, \tag{1}$$

which may also be considered a characteristic inverse length scale of the microstructure. Another definition is the ratio of the interface area A to the sample volume V containing both solid and liquid phases

$$S_v = A/V = f_s S_s, \tag{2}$$

where $f_s = V_s/V$ is the solid volume fraction. S_v is also referred to as the interfacial area density. S_s and S_v can be measured directly from metallographic sections. Both quantities are key ingredients in volume-averaged (macroscopic) models of alloy solidification and are needed, for example, in modeling of microsegregation (back-diffusion) or melt flow through the mush [3].

In the latter example, the permeability of the mush K_p is directly related to the interfacial area density via the Kozeny-Carman relation $K_p \propto (1-f_s)^3/S_v^2$.

Under isothermal conditions, the evolution of the inverse specific interface area S_s^{-1} is usually described by the following relation for surface energy driven coarsening [1]

$$S_s^{-n} - S_{s0}^{-n} = Kt \tag{3}$$

or

$$S_s^{-1} = \left(S_{s0}^{-n} + Kt\right)^{\frac{1}{n}}, \tag{4}$$

where t, n, S_{s0}, and K are time, coarsening exponent, specific interface area at $t = 0$, and coarsening rate constant, respectively. For volume diffusion-limited coarsening an exponent of $n = 3$ has been firmly established by both experiments and theory. This exponent was first obtained in the context of Ostwald ripening by the LSW theory [4, 5, 6], describing the long-time evolution of a system of dispersed spherical particles. While the LSW theory assumes an idealized geometry and vanishing solid fractions, it has been possible to extend the validity of $n = 3$ to more general geometries [1, 7] and higher solid fractions [8], including morphologies that are initially dendritic. In the latter case, the coarsening rate constant K is known to be a strong function of the solid fraction [8]. While in pure coarsening theories the solid fraction is assumed to remain constant, a model has been developed for the case of concurrent growth and coarsening [9]. While this model is limited to low solid fractions, an exponent of $n = 3$ was obtained even in the presence of solidification.

In contrast to pure coarsening, solidification implies that the solid fraction f_s increases over time. Eventually, the specific interface area becomes strongly affected by coalescence and the theory of Ref. [9] is no longer valid. For processes that involve only growth, but no surface energy driven coarsening, the interfacial area density S_v is often correlated to f_s by

$$S_v = C f_s^p \left(1 - f_s\right)^q, \tag{5}$$

where C, p, and q are constants. According to Eq. (5), S_v experiences a steep increase during growth, goes through a maximum, and then decreases due to impingement and coalescence of interfaces. Different values for the exponents p and q have been suggested in the literature. Speich and Fisher [10] found that data from a broad range of recrystallization experiments could be described by $p = q = 1$. These exponents were later confirmed by a computational model for the growth and impingement of grains [11]. Other suggestions have been $p = q = 2/3$ [12] and $p = q = 1/2$ [13]. A geometrical model of growing and impinging spheres has demonstrated that the parameters C, p, and q are influenced by the nucleation kinetics and the spatial distribution of the spheres [14]. Hence, generally valid values for C, p, and q are unavailable.

In summary, Eqs. (4) and (5) are useful relations for the specific interface area, but are limited to seemingly opposing cases. While Eq. (3) was developed for the isothermal case ($\dot{\theta} = 0$, f_s =const), where the interface area evolves over time due to coarsening, Eq. (5) is meant to describe situations where f_s varies with time due to growth ($\dot{\theta} \neq 0$, $f_s \neq$const) but the interface area does not change when the solid fraction is held constant. Hence, the question remains how these two models can be combined for situations that involve both growth and coarsening, such as dendritic solidification of alloys.

The direct measurement of the specific interface area during alloy solidification has not been possible until about a decade ago. Now, high-speed X-ray tomography is able to provide time-resolved geometric data during metallic alloy solidification [15, 16]. In addition, recent advancements in computational methods allow for detailed studies of solidification using phase-field simulations. The present work uses a 3D phase-field model to analyze concurrent growth and coarsening during directional solidification of a binary alloy. Experimental data for the

specific interface area are extended to cooling rates that are beyond the limit of present X-ray tomography. As a result, we are able to show how the specific interface area kinetics change with cooling rate.

2. Model

To analyze the morphological evolution during growth and coarsening we use a three-dimensional phase-field model of a columnar dendrite (Al-6wt.%Cu). The model setup corresponds to a Bridgman experiment, where dendrites grow in a fixed temperature gradient G that moves at constant velocity V_p. We employ a phase-field model for directional solidification of a binary alloy, based on the frozen gradient approximation of the temperature field, that is discussed in detail in [17]. The model is extended to include finite-rate solute diffusion in the solid [18].

The numerical implementation of the problem is based on the FEM library AMDiS [19, 20], which enables the use of adaptive mesh refinement and efficient parallelization on a HPC infrastructure. A semi-implicit time integration scheme is employed to allow for adaption of the time steps to the different time scales of the interface dynamics during growth and coarsening. The present simulation is for a pulling speed of $V_p = 300\,\mu\text{m/s}$ and temperature gradient of $G = 200\,\text{K/cm}$. The material data are representative of an Al-Cu alloy and are given by an alloy solute concentration $c_0 = 6\,\text{wt.\%}$, liquidus slope $m = -2.6\,\text{K/wt.\%}$, partition coefficient $k = 0.14$, and mass diffusivities in the liquid $D_l = 3000\,\mu\text{m}^2/\text{s}$ and solid $D_s = 0.3\,\mu\text{m}^2/\text{s}$, respectively. The capillary length is taken as $d_0 = 0.005\,\mu\text{m}$ and the surface energy anisotropy coefficient as $\varepsilon_4 = 0.02$. The computational domain covers a 1/8 sector of a full dendrite by using available symmetries. The width of the simulation domain is 70 µm, i.e. one half of the primary dendrite spacing, while the length is 350 µm. No-flux conditions are applied on all boundaries and the initial geometry of the seed at the bottom of the domain is a parabola of revolution. The domain is limited at the top, such that the dendrite tip impinges on the upper wall, and the simulation proceeds by further solidification and coarsening of the previously grown structure (see Fig. 1). Numerical and phase-field parameters were chosen in order to obtain converged results for the steady state dendrite tip undercooling. This value was then used as the initial liquid undercooling in the present simulation. The computations were performed on a HPC cluster using 512 CPU's and took about one week of time. The smallest element size was 0.153 µm and the average problem size was 2.5×10^7 degrees of freedom.

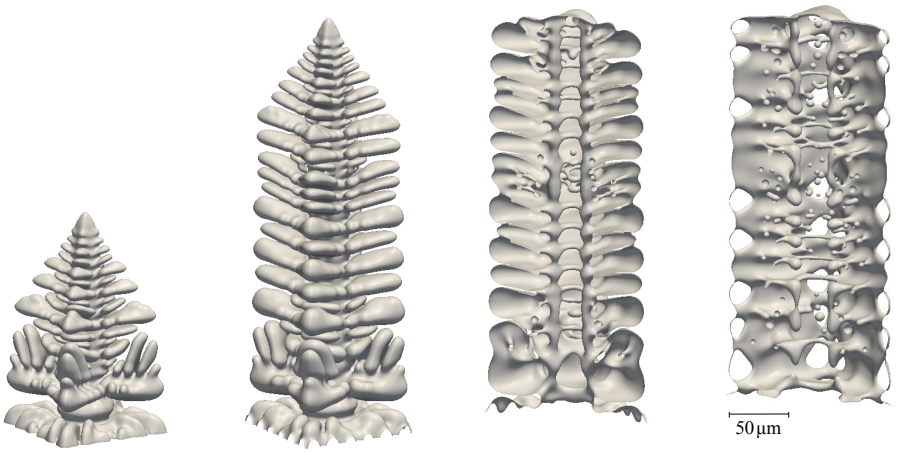

(a) $t = 0.5\,\text{s}$ (b) $t = 1\,\text{s}$ (c) $t = 2.5\,\text{s}$ (d) $t = 7\,\text{s}$

Figure 1: Evolution of the dendrite geometry: (a)-(b) full view of the growing dendrite, (c)-(d) cutaway view of half of the dendrite during the coarsening stage.

3. Results and discussion

Fig. 1 shows snapshots of the computed dendrite at different times. The first stage is characterized by a rapid increase of the interface area, while at later times coarsening and coalescence of sidebranches can be observed. At high solid fractions, liquid channels and inclusions are formed inside the solid structure (Figs. 1c, 1d).

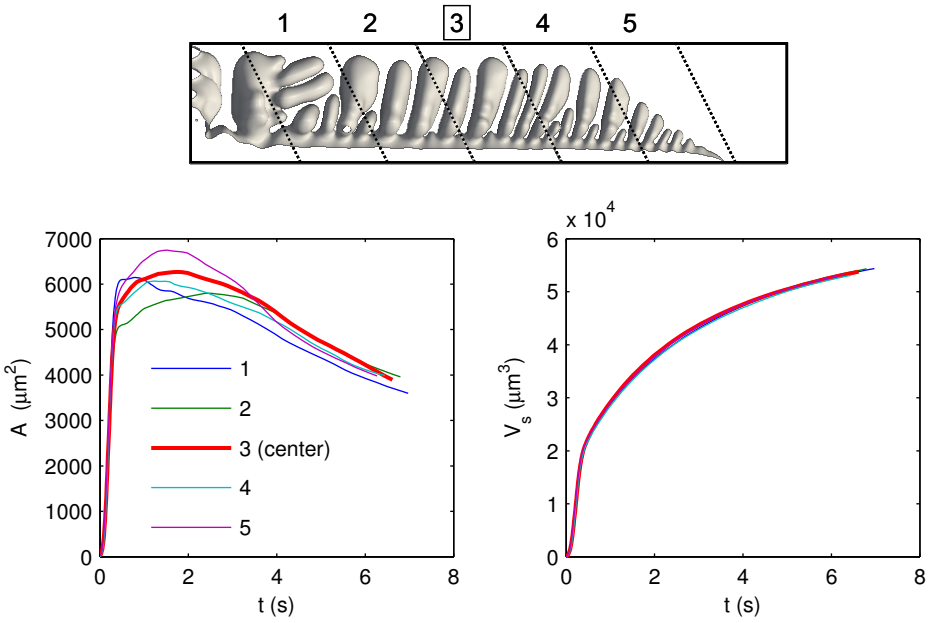

Figure 2: Averaging volumes at different positions along the growth direction (top), and evolution of the averaged interface area and solid volume (bottom).

For the evaluation of the interface area A and the solid volume V_s of the dendrite shown in Fig. 1, five sample volumes are placed along the direction of growth inside the computational domain; see Fig. 2 (top). The size of the sample volumes is chosen small enough to neglect temperature variations within them, but large enough to avoid excessive scatter in the integral measures. The tilted shape of the sample volumes further aids in suppressing scatter by covering an approximate constant number of sidebranches between adjacent volumes. The interface area A and solid volume V_s for each sample volume are plotted in Fig. 2 (bottom) as a function of time, where $t = 0$ refers to the instant when a portion of the interface enters the sample volume. It can be seen that A differs more strongly between the five sample volumes than V_s. The center sample volume is most representative of the average variation in A and is used exclusively in the following analysis.

A scaled undercooling and cooling rate can be defined, respectively, as

$$\theta = \frac{T_l(c_0) - T}{\Delta T_0}, \qquad \dot{\theta} = \frac{-\dot{T}}{\Delta T_0}, \tag{6}$$

where T is the temperature, $\dot{T}$ is the cooling rate, $T_l(c_0) = T_m - |m|c_0$ is the equilibrium liquidus temperature and $\Delta T_0 = |m|c_0(1/k - 1)$ is the equilibrium freezing range. Figure 3 shows the computed solid fraction as a function of the scaled undercooling. As expected, the solid fraction is equal to zero until the scaled undercooling reaches the dendrite tip undercooling ($\theta \approx 0.04$); afterwards, the solid fraction increases sharply with increasing scaled undercooling. This solid fraction variation can be compared to the classical lever rule and Scheil equation predictions,

which assume that the dendrite tips are located at the equilibrium liquidus isotherm ($\theta = 0$). In terms of the present nomenclature, the lever rule and the Scheil equation are given, respectively, by

$$f_s = \left[1 + k\left(\frac{1}{\theta} - 1\right)\right]^{-1} \qquad \textit{(lever rule)} \tag{7}$$

and

$$f_s = 1 - \left[1 + \theta\left(\frac{1}{k} - 1\right)\right]^{\frac{1}{k-1}} \qquad \textit{(Scheil equation)}. \tag{8}$$

The above equations can also be written in time-dependent form $f_s(t)$ by using the relation $\theta = \dot{\theta}t$, where it is assumed that $T(t = 0) = T_l(c_0)$. Figure 3 shows that, other than for the dendrite tip undercooling effect, the lever rule and the Scheil equation closely bound the $f_s(\theta)$ variation from the phase-field simulation.

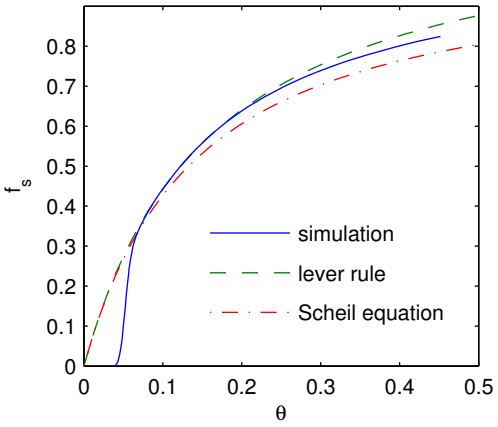

Figure 3: Solid fraction as a function of the scaled undercooling.

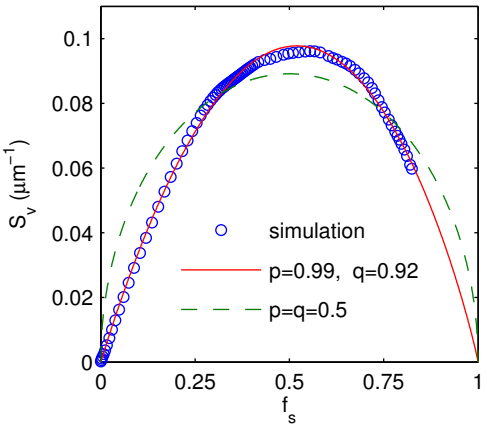

Figure 4: Variation of the interfacial area density with solid fraction.

The computed interfacial area density S_v is plotted in Fig. 4 against the solid fraction. The figure shows that S_v varies in accordance with Eq. (5). By fitting the present data to Eq. (5), it is found that the exponents are equal to $p = 0.99$ and $q = 0.92$, which is close to $p = q = 1$ suggested in Ref. [10]. Clearly, exponents of $p = q = 1/2$ [15] do not fit the simulation results.

The various temporal evolutions of the inverse specific interface area S_s^{-1} are shown and compared in Fig. 5. Figures 5a, 5b, and 5c represent experimental data from three different studies [21, 16, 15], while Fig. 5d provides the results for the present simulation. The plots are ordered by increasing cooling rate. The experimental data for S_s are fit to Eq. (4) in order to determine the exponent n. For a vanishing cooling rate ($\dot{\theta} = 0$), Fig. 5a indicates that the value of $n = 3$ that is expected for pure coarsening is approximately attained. The exponent decreases with increasing cooling rate. For the present simulation with the highest cooling rate (Fig. 5d), an exponent of $n = 3$ is obtained for short times ($t < 2\,\mathrm{s}$), while an exponent of $n = 0.86$ fits the simulation data at longer times ($t > 2\,\mathrm{s}$). The exponent of $n = 3$ during the initial growth stage is in agreement with the finding in Ref. [9] for concurrent growth and coarsening of spheres in the limit of low solid fractions. The solid fraction at $t = 2\,\mathrm{s}$ is equal to 0.5, indicating that the neglect of coalesence of solid is only appropriate up to this fraction. The exponent of $n = 0.86$ observed at higher solid fractions ($t > 2\,\mathrm{s}$) may be explained as follows. By inserting the Scheil equation, Eq. (8), into Eq. (5), assuming that $p = q = 1$ and using $S_s^{-1} = f_s/S_v$, an analytical

relation for the inverse specific interface area as a function of time can be derived as

$$S_s^{-1} = \frac{1}{C}\left[1 + \dot{\theta}t\left(\frac{1}{k} - 1\right)\right]^{\frac{1}{1-k}}. \tag{9}$$

Comparing this relation to the general coarsening law given by Eq. (4) gives

$$n = 1 - k, \tag{10}$$

where $k = 0.14$ in the present simulation. Figure 5d shows that an exponent of $n = 0.86$ does indeed provide a good fit of the predicted S_s^{-1} at long times. Note that this derivation is only valid for $p = q = 1$ and cannot be applied to the data in Figs. 5b and 5c.

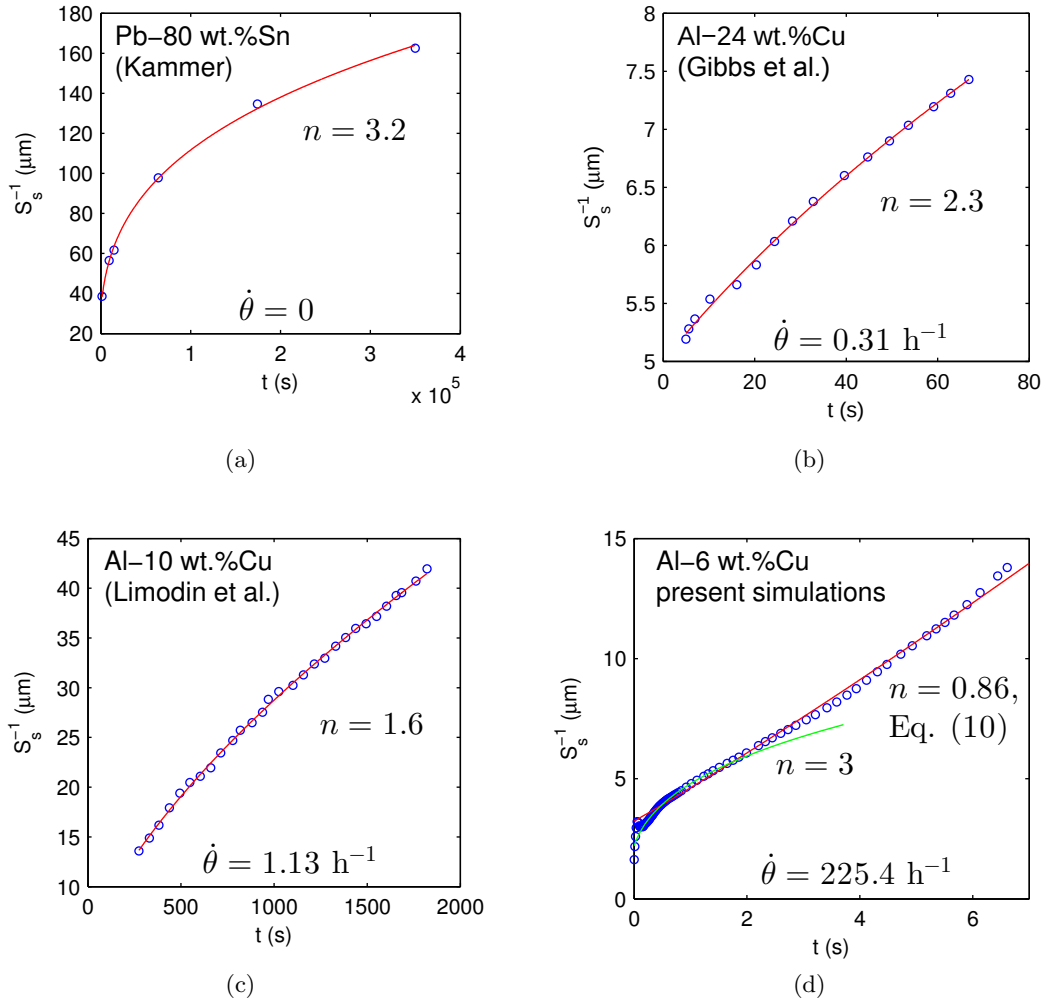

Figure 5: Evolution of the characteristic length scale for increasing scaled cooling rates: experimental data from the dissertation of D. Kammer [21] (a), personal communication with P. Voorhees [16] (b), and Limodin et al. [15] (c); (d) shows the present simulation results.

4. Conclusions

In this work we have studied the kinetics of the solid-liquid interface of a columnar dendrite by performing a 3D phase-field simulation. The computed interface area and volume are integrated

over a representative volume element and presented in terms of the inverse specific interface area as a function of time and the interfacial area density as a function of solid fraction. These results are compared to existing models for pure coarsening and pure growth. For the latter case, Eq. (5), exponents close to $p = q = 1$ are obtained, which compares favorably with the exponents suggested by Speich and Fisher [10]. Comparing the present data to a pure coarsening law, Eq. (4), gives an exponent of $n = 3$ at short times and $n = 0.83$ at longer times. The former is in agreement with the concurrent growth and coarsening theory of Ref. [9], while the latter is explained in the special case of $p = q = 1$ and the solid fraction following the Scheil equation. An examination of previous experimental data, together with the present simulation results, reveals that the coarsening exponent decreases with increasing cooling rate. Nonetheless, considerable additional research is necessary to obtain a generally valid relation for the evolution of the specific interface area in alloy solidification. Simulations are underway that investigate the effect of different cooling rates and other alloy characteristics on the interface kinetics.

Acknowledgments

This work was financially supported by the Helmholtz alliance Limtech and NASA (NNX10AV35G and NNX14AD69G). We thank the supercomputing center in Jülich (HDR08) for providing computing time.

References

[1] Marsh S and Glicksman M 1996 *Metall Mater Trans A* **27** 557–567 ISSN 1073-5623
[2] Mendoza R, Alkemper J and Voorhees P 2003 *Metall Mater Trans A* **34** 481–489 ISSN 1073-5623
[3] Ni J and Beckermann C 1991 *Metall Trans B* **22** 349–361 ISSN 0360-2141
[4] Lifshitz I and Slyozov V 1961 *J Phys Chem Solids* **19** 35–50 ISSN 0022-3697
[5] Wagner C 1961 *Z Elektrochem* **65** 581–591
[6] Voorhees P 1992 *Annu Rev Mater Sci* **22** 197–215 ISSN 0084-6600
[7] Mullins W 1986 *J Appl Phys* **59** 1341–1349 ISSN 0021-8979
[8] Marsh S and Glicksman M 1996 *Acta Mater* **44** 3761–3771 ISSN 1359-6454
[9] Ratke L and Beckermann C 2001 *Acta Mater* **49** 4041–4054 ISSN 1359-6454
[10] Speich G; Fisher R 1966 *Recrystallization, grain growth and textures* (ASM, Materials Park, OH)
[11] Price C 1987 *Acta Metall Mater* **35** 1377–1390 ISSN 0001-6160
[12] Cahn J 1967 *T Metall Soc Aime* **239** 610–& ISSN 0543-5722
[13] Ratke L and Genau A 2010 *Acta Mater* **58** 4207–4211 ISSN 1359-6454
[14] Almansour A, Matsugi K, Hatayama T and Yanagisawa O 1996 *Mater T Jim* **37** 1595–1601 ISSN 0916-1821
[15] Limodin N, Salvo L, Boller E, Suery M, Felberbaum M, Gailliegue S and Madi K 2009 *Acta Mater* **57** 2300–2310 ISSN 1359-6454
[16] Gibbs J, Mohan K, Gulsoy E, Shahani A, Xiao X, Bouman C, De Graef M and Voorhees P 2015 (to be published)
[17] Echebarria B, Folch R, Karma A and Plapp M 2004 *Phys. Rev. E* **70** 061604
[18] Ohno M and Matsuura K 2009 *Phys Rev E* **79** 031603
[19] Voigt A and Witkowski T 2012 *Journal Of Computational Science* **3** 420–428 ISSN 1877-7503
[20] Witkowski T 2013 *Software concepts and algorithms for an efficient and scalable parallel finite element method* Ph.D. thesis Technische Universität Dresden
[21] Kammer D 2006 *Three-dimensional analysis and morphological characterization of coarsened dendritic microstructures* Ph.D. thesis Northwestern University